MeV ion irradiation-induced creation and relaxation of mechanical stress in silica

E. Snoeks,[a] T. Weber,[b] A. Cacciato,[c] and A. Polman
FOM Institute for Atomic and Molecular Physics, Kruislaan 407, 1098 SJ Amsterdam, The Netherlands

In situ wafer curvature measurements were performed to study mechanical stress in amorphous SiO_2 during Xe, Ne, and Er ion irradiation at energies in the 0.27–4.0 MeV range. Three phenomena are observed: network compaction, radiation-induced viscous flow, and a nonsaturating anisotropic deformation phenomenon. The radiation-induced *viscosity* is shown to be inversely proportional to the energy density deposited into atomic displacements. The relation between radiation-induced flow and diffusion is discussed in the context of the Stokes–Einstein relation. Viscous flow serves to relax stress, yet a continuous nonsaturating *anisotropic deformation* effect causes the stress in the irradiated layer to saturate at nonzero values: Xe irradiation at an energy below 3.6 MeV results in a tensile saturation stress; for higher energies a compressive stress builds up. These effects are explained in terms of competing bulk and surface deformation processes resulting from local heating of the SiO_2 around the ion tracks. The macroscopic effect of deformation phenomena is illustrated by showing the surface morphology after 4.9 MeV Er irradiation of silica through a contact implantation mask. Finally, an *in situ* stress study of an alkali borosilicate glass is presented. In this case a fourth radiation induced effect is observed, namely, the generation and annihilation of volume occupying point defects. These defects are shown to anneal out at room temperature, following a broad spectrum of activation energies. © *1995 American Institute of Physics.*

I. INTRODUCTION

The effect of ion irradiation on the structure of silica glass has been studied for many years.[1,2] Most of these studies involve irradiation energies up to several hundred keV. More recently, investigations using extremely high-energy (~100 MeV) irradiation were reported.[3,4] The intermediate energy range (~MeV), however, has not been explored. This range is important in, for example, ion implantation of optical waveguide materials, where MeV energies are needed to reach the required implantation depths of 2–5 μm.[5–7] It is therefore important to study the response of silica to irradiation at these MeV energies.

Until now, three different radiation-induced deformation phenomena are known in SiO_2: densification,[1,8] radiation-enhanced viscous flow,[9–11] and an anisotropic deformation phenomenon.[3,11] The origin of densification of amorphous SiO_2 is well known.[1,2,8] Atomic collisions cause the SiO_2 ring network to rearrange into smaller, compacter rings. The density increase eventually saturates with fluence. Densification results in a tensile stress if the irradiated region is constrained by a substrate.

Less is known about radiation-enhanced viscous flow. Primak first suggested that stress in SiO_2 can relax viscously at room temperature under H and He irradiation.[9] Later Volkert and Polman demonstrated with *in situ* wafer bending measurements that such radiation-enhanced plastic flow in SiO_2 is Newtonian,[10] i.e., the strain rate is proportional to the stress. The nature of the defects that cause radiation-

enhanced viscous flow, and their creation and annihilation processes are investigated in this article.

Another manifestation of irradiation-induced atomic transport is ion-beam mixing. This phenomenon has been investigated for a number of years,[12–14] and is described using a radiation-induced diffusion coefficient. In this article the relation between radiation-induced flow and diffusion is discussed in terms of a radiation-induced analogue of the Stokes–Einstein relation.[15]

Our earlier work has shown that a thin-film silica implantation mask collapses completely after irradiation with 1×10^{16} Xe/cm^2 at 4.0 MeV.[11] This is due to an anisotropic deformation effect, which is attributed to the high deposited energy density (~2.3 keV/nm electronic and 0.8 keV/nm nuclear energy loss). An anisotropic deformation process was also observed during irradiation of thin bulk materials with ions at very high energies (up to 360 MeV) such that the particle range was much higher than the sample thickness, and electronic energy loss was the only stopping process.[3,4] The nature and energy dependence of this deformation phenomenon is studied in this article for MeV ion irradiation of SiO_2 films on Si substrates. *In situ* measurements of the sample curvature during irradiation are used to determine the stress in the irradiated SiO_2. A large *compressive* saturation stress builds up after 6×10^{13} Xe/cm^2 at 4.0 MeV. For energies of 3.5 MeV and lower, a surprising result is obtained: a *tensile* saturation stress is observed. This indicates that an anisotropic deformation with opposite effect occurs.

Measurements are also performed on alkali borosilicate glass. In addition to the three effects described above (densification, viscous flow, and anisotropic deformation) we find evidence for the creation and room-temperature annihilation of defects that are not related to the defects causing flow.

Finally, the macroscopic effect of the deformation phenomena is illustrated using measurements on sodalime silicate glass that had been implanted with 4.9 MeV Er ions through a Au contact mask. Optical microscopy and surface profilometry reveal a dramatic change in the surface morphology, which can be explained by the same mechanisms as described above.

II. EXPERIMENT

In situ wafer curvature experiments were performed both on SiO_2 films on a Si substrate, and on commercially available sodalime borosilicate microscope cover slides (Chance CM5, 150 μm thick). The SiO_2 films, 1.85 μm thick, were obtained by wet thermal oxidation of double-sided polished, undoped, (100) Si wafers of 100 μm thickness at 1100 °C. Rectangular pieces (5×25 mm^2) were clamped at one end to a copper block, leaving the other end free to bend. A He-Ne laser beam was scanned up and down on the back of the sample while the sample was implanted from the front.[16] From the angle of the reflected beam the radius of curvature was determined during irradiation. In order to obtain measurable reflection from the transparent sodalime borosilicate, a ~20 nm Al layer was evaporated on the backside.

When the thickness of the region modified by the ion beam (t_{ion}) is much smaller than the thickness t_s of the substrate, the integrated in-plane stress S can be calculated from the measured radius of curvature R using the biaxial elastic modulus Y_s of the substrate

$$S = \int_0^{t_{ion}} \sigma(x)dx = \frac{Y_s t_s^2}{6R}. \tag{1}$$

Here, $\sigma(x)$ is the local in-plane stress at a depth x. For the (100) Si substrate underneath the SiO_2 film we use $Y_s = 181$ GPa,[17] while for the bulk sodalime borosilicate glass $Y_s = 90$ GPa was used.[18] In this article, positive stress values refer to compressive stress, and negative values to tensile stress. Deviations of the laser beam due to the vacuum view-port and mirrors limited the resolution of the integrated stress measurements to ±5 N/m. However, local variations in wafer and oxide thickness limit the absolute determination of the integrated stress to ±15 N/m. The *average* stress (σ, in Pa) in the irradiated region is obtained from the measured *integrated* stress (in N/m) by $\sigma = S/t_{ion}$. The average in-plane elastic strain ϵ can then be calculated from the in-plane stress using the biaxial elastic modulus Y_{ion} of the implanted region $\epsilon = \sigma/Y_d$. In the case of pure SiO_2, $Y_{ion} = 100$ GPa was used. The thickness of the ion-beam damaged layer t_{ion} is taken to be the projected ion range plus the half width at half maximum of the implantation profile. The choice of this definition causes a systematic error in the estimate of the average stress, which we included in the error bars in figures that are presented in this article.

Irradiations were done with Ne, Er, and Xe at room temperature with energies ranging from 260 keV to 4.0 MeV. The ion beam was electrostatically scanned through a 27×27 mm^2 aperture, so that the full width of the sample was irradiated. The maximum ion current density was 20 nA/cm^2. Ion ranges and SiO_2 film thickness were determined with
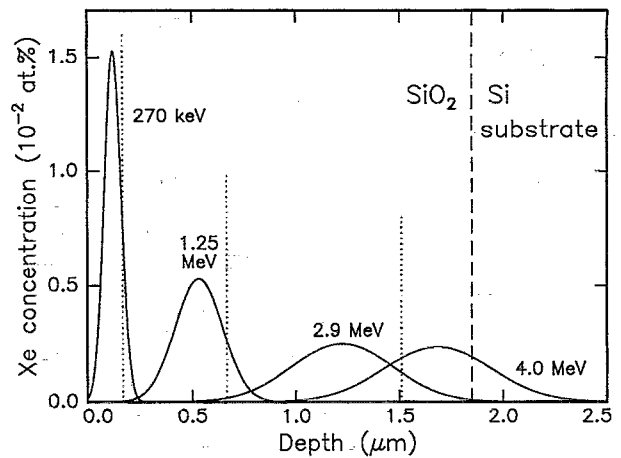

FIG. 1. Xe concentration profiles in SiO_2 on Si after implantation to 1.0×10^{14} Xe/cm^2 at energies of 0.270, 1.25, 2.90, and 4.0 MeV. The lines are Gaussian fits to the data obtained by 4.0 MeV ^{4}He$^+$ RBS. The SiO_2 film is 1.85 μm thick. The thickness t_{ion} of the ion beam modified regions (defined in text) are indicated by dotted vertical lines.

Rutherford backscattering spectrometry (RBS) using 2.0 and 4.0 MeV ^{4}He$^+$, and scattering angles of 169° and 160°, respectively. Monte Carlo code TRIM'89 was used to calculate nuclear and electronic energy loss.[19]

Finally, commercially available 1-mm-thick sodalime silicate glass (Fisher Premium) was implanted with 4.9 MeV Er at room temperature to a fluence of 3×10^{16}/cm^2, using a gold thin-film implantation contact mask with 15-μm-wide etched trenches. After irradiation, the glass surface was studied with optical microscopy and Taly step surface profiling.

III. PURE SiO$_2$

A. Results

First we will present measurements on the SiO_2 films on Si, irradiated with Xe at 0.27, 1.25, 2.9, and 4.0 MeV. Figure 1 shows the Xe concentration profiles for a fluence of 1×10^{14}/cm^2. Because of the noise level of the data measured by RBS, we show only the Gaussian profiles that fit the data. As can be seen, in all cases the Xe concentration is lower than 150 ppm, so that volume changes due to the implanted ions can be excluded for such fluences. The oxide thickness (t_{ox}) was determined to be 1.85 μm. The ion modified region (t_{ion}) extends from the surface to the dotted lines, indicated for each energy. Some of the 4.0 MeV Xe ions have entered the Si substrate.

Figure 2(a) shows the integrated stress of the SiO_2 films during Xe irradiation as a function of fluence, for different energies. As can be seen, the initial integrated stress before irradiation is $S_0 = 580 \pm 15$ N/m, i.e., compressive. This corresponds to an average elastic strain in the SiO_2 film of 3.1×10^{-3}, and originates from the difference in thermal contraction between the SiO_2 and the Si substrate, upon cooling down from 1100 °C to room temperature after thermal oxidation. The curves in Fig. 2(a) are a result of ion-beam-induced stress changes, superimposed on a background stress from strained SiO_2 which lies deeper than the irradiated region. This background is equal to $S_0(t_{ox} - t_{ion})/t_{ox}$. By sub-
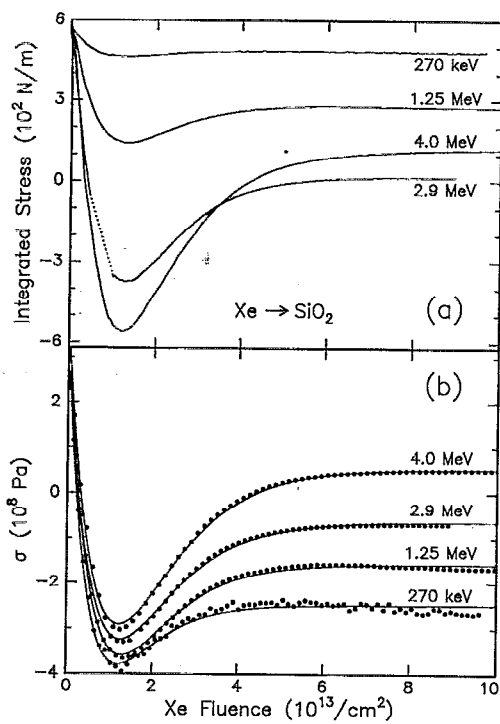
Snoeks *et al.*

FIG. 2. (a) Integrated stress in 1.85-μm-thick SiO_2 films on Si(100) during Xe irradiation at room temperature, as function of Xe fluence. *In situ* measurements are shown for beam energies ranging from 0.27 to 4.0 MeV, all at constant Xe flux of 3.1×10^{10} ions/cm² s. (b) The same data represented as average stress in the ion-beam modified layer (solid data points). The solid lines are fits using Eq. (3).

tracting the background and dividing by t_{ion}, the data in Fig. 2(a) can be converted to an average stress in the ion-beam damaged layer [Fig. 2(b)]. In this way, curves for different irradiation energies can be compared directly. As can be seen in Fig. 2(b), the initial average local stress is 3.0×10^8 Pa and is identical for all samples. After the ion irradiation is started, the stress first decreases, and becomes tensile. At a fluence of about 1.2×10^{13} Xe/cm², the stress reaches a minimum, for higher fluences it starts to increase again and eventually saturates. The saturation stress depends on the irradiation energy, and varies from $-(2.6 \pm 0.3) \times 10^8$ Pa (tensile) at 270 keV, to $+(0.45 \pm 0.06) \times 10^8$ Pa at 4.0 MeV (compressive). Similar saturation stresses are also observed in bulk silica glass, where no background subtraction was necessary, as will be shown in Sec. IV.

Figure 1 shows that for the 4.0 MeV Xe irradiation some of the ions have entered the Si substrate. Indeed, channeling RBS showed that a 0.18-μm-thick Si layer was damaged near the SiO_2/Si interface. This gives a small positive contribution to the measured integrated stress,[16] which was determined by measuring the curvature after etching the SiO_2 layer from the substrate after irradiation. It was found that this Si contribution was less than 30 N/m (0.16×10^8 Pa) in the saturation stress, and in Fig. 2(b) this contribution was subtracted from the 4.0 MeV data as a linearly increasing background.[16]

All reported curves are independent of ion flux (not shown), at least between 0.9 and 3.1×10^{10}/cm² s, indicating that there is no interaction between individual ion-damaged

regions. When the ion beam was switched off at any point during the experiment, the stress remained unchanged.

Similar measurements were performed using Ne and Er ions at various energies. Qualitatively, the stress during irradiation showed the same behavior as described above. In the next section, these additional measurements will be used to obtain quantitative information on the stress creation and relaxation mechanisms.

B. Analysis

As was shown in a previous letter,[11] the general behavior in Fig. 2 can be described by a model that contains three basic mechanisms: *densification*, radiation-enhanced *plastic flow*, and an *anisotropic deformation* mechanism. The rate equation for the average in-plane stress in the irradiated region with respect to fluence ϕ is

$$\frac{d\sigma}{d\phi} = Y_{ion}\left(\frac{d\epsilon_p}{d\phi} + A\right) - \frac{Y_{ion}}{6\eta_{rad}}\sigma. \tag{2}$$

Here, Y_{ion} is the biaxial elastic modulus of the irradiated layer, ϵ_p the elastic strain due to density changes, and A the anisotropic deformation rate. Viscous flow is described by a term negatively proportional to the stress and inversely proportional to η_{rad}, the radiation induced viscosity defined as $\eta_{rad} = \dot{\phi}\eta$, where η is the viscosity, and $\dot{\phi}$ is the ion flux. In this definition of η_{rad}, the areal density of incoming ions replaces the time unit which appears in the thermal viscosity η.[10,16] Note that the lower the viscosity, the "softer" the material. It is assumed that η_{rad} is constant during the irradiation. It is further assumed that densification is described by a damage overlap model,[1,8] in which the strain due to densification (from ρ to $\rho + \Delta\rho$) goes exponentially from zero to $\epsilon_{sat} = -\Delta\rho/3\rho$, i.e., $\epsilon_p(\phi) = \epsilon_{sat}[1 - \exp(-\phi/\phi_\rho)]$, with ϕ_ρ a characteristic fluence for densification. The anisotropic deformation rate A is independent of both ϕ and σ, and thus introduces a continuous source for stress. Using these assumptions, the solution of Eq. (2) is

$$\sigma(\phi) = (\sigma_0 - \sigma_{sat} + D)\exp\left(-\frac{Y_{ion}}{6\eta_{rad}}\phi\right)$$
$$- D\exp(-\phi/\phi_\rho) + \sigma_{sat}, \tag{3}$$

in which $D = 6Y_{ions}\epsilon_{sat}\eta_{rad}/(6\eta_{rad} - Y_{ion}\phi_\rho)$, and σ_0 and σ_{sat} are initial and final saturation stress, respectively. The latter is determined by the product of A and η_{rad}: $\sigma_{sat} = 6A\eta_{rad}$.

The drawn lines in Fig. 2(b) are fits according to Eq. (3). The fits describe the data quite well. The fit parameters for $\Delta\rho/\rho$ (which follows from ϵ_{sat}), ϕ_ρ, η_{rad}, and A are plotted in Fig. 3 as a function of irradiation energy. Note that the error in the determination of σ owing to the choice of t_{ion} does not contribute to the error in η_{rad} and ϕ_ρ. The only parameter that strongly depends on irradiation energy is the deformation rate A. The parameters for densification and the radiation-induced viscosity are almost independent on the Xe energy. We will now discuss these four parameters in more detail.
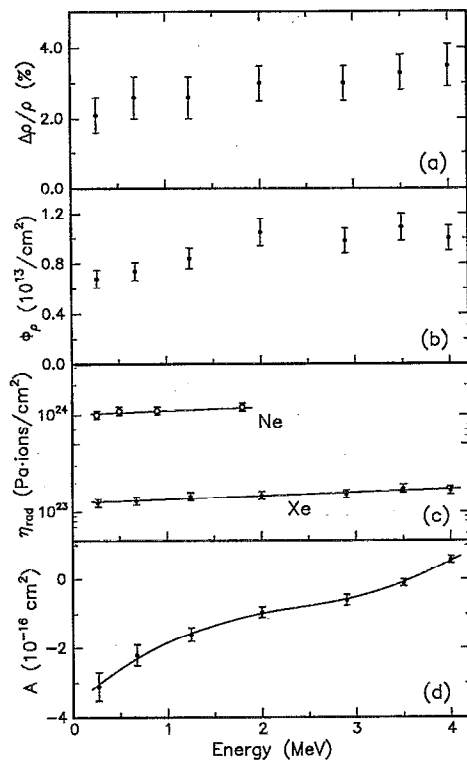
FIG. 3. Fit parameters from Eq. (3) for the data in Fig. 2(b), as a function of Xe irradiation energy (filled data points): (a) density increase, (b) characteristic fluence for densification, (c) radiation-induced viscosity, and (d) anisotropic deformation rate. The radiation induced viscosity during Ne irradiation of SiO_2 (circles) is included in (c).

C. Discussion

1. Densification

The amount of densification [Fig. 3(a)] is in the range 2%–3.5%. This agrees well with previously established values.[1,2,8,20] The characteristic fluence for densification is found to be $\phi_\rho = (0.7-1.1) \times 10^{13}$ ions/cm² for the Xe irradiations [Fig. 3(b)]. For (0.26–1.8 MeV) Ne and 3.0 MeV Er irradiations, $\phi_\rho = (7.3 \pm 1.0) \times 10^{13}$ and $(0.8 \pm 0.1) \times 10^{13}$ ions/cm² were found, respectively. In all cases, the total energy deposited in atomic collisions at the fluence ϕ_ρ is $(1.4 \pm 0.2) \times 10^{20}$ keV/cm³, independent of the ion (Ne, Xe, or Er).[19] This also agrees with previous work, which has shown that the typical energy density required to saturate volume changes in silica is $\sim 10^{20}$ keV/cm³.[1,2,8]

2. Radiation-enhanced viscous flow

The values for the Xe irradiation-induced viscosity η_{rad} are plotted in Fig. 3(c) (solid data points). As can be seen, η_{rad} is roughly 1.5×10^{23} Pa ions/cm², almost independent of irradiation energy in the 0.27–4.0 MeV range. The electronic energy loss varies by a factor of 4 over this energy range, whereas the nuclear energy loss, which is of the same order of magnitude, remains almost constant over this energy range. Therefore, it is concluded that the defects introduced by electronic excitations do not contribute strongly to the viscosity, and that atomic displacements via nuclear collisions are dominantly responsible for radiation enhanced flow.
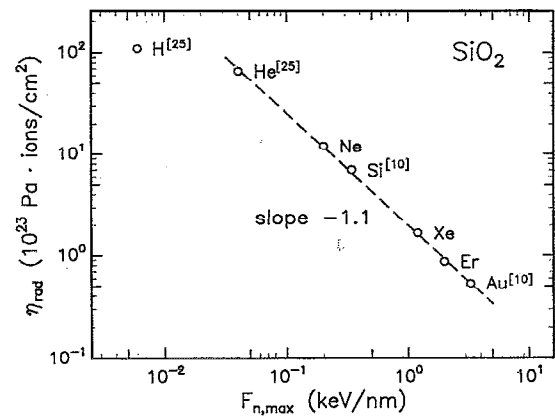

FIG. 4. Radiation-induced viscosity as a function of maximum energy density deposited by nuclear collisions, both plotted on logarithmic scales. Data for Ne, Xe, and Er are from this work, data for Si and Au are derived from Ref. 10, and data for H and He are taken from Ref. 25.

Additionally, Fig. 3(c) shows η_{rad} determined for Ne irradiated SiO_2 at energies in the range 0.26–1.8 MeV. The maximum nuclear energy loss for the Ne irradiations is roughly ten times lower than for Xe. Indeed the value of η_{rad} is almost ten times higher, and again almost independent of energy.

Figure 4 summarizes the measured radiation induced viscosity η_{rad} in SiO_2 as a function of the maximum nuclear energy loss $F_{n,max}$, for different ions. The values for Ne, Xe, and Er are determined in this work. Wafer curvature data for Si and Au were taken from Ref. 10 and analyzed using Eq. (3). From this figure it is clear that η_{rad} decreases (i.e., the SiO_2 becomes more soft) with increasing nuclear energy loss (or ion mass).

The dashed line in Fig. 4 is a linear fit through the data. The slope is -1.1, showing that the radiation-induced viscosity is almost inversely proportional to the nuclear energy loss. In the remainder of this subsection we will use this knowledge to consider details on the atomic mechanism for radiation induced viscous flow. Earlier work has shown that there is no ion-flux dependence of η_{rad}. Therefore, there is no interaction between subsequent collision cascades and flow occurs due to defects created within single collision cascades.[10] Thus, the macroscopically defined η_{rad} is a result of a space-time average of the viscosity of SiO_2 at room temperature containing isolated fluid-like spikes. Viscosity is generally described as inversely proportional to the concentration of defects that contribute to viscous flow (flow defects).[21–23] In the ion-beam case it is important to know the number of flow defects generated per unit length as well as the defect annihilation rate in the cascade. Before any defects have annihilated, the number of flow defects per unit length is proportional to the nuclear energy loss. The experimental result from Fig. 4 is that the averaged viscosity is inversely proportional to the number of flow defects created per unit length. This implies that the defect annihilation rates must be the same in all cascades that were used in Fig. 4. To understand this, two cases can be distinguished. (1) The annihilation mechanism is unimolecular. In this case the characteristic lifetime of flow defects is indeed constant. (2) The

annihilation mechanism of flow defects is bimolecular, as is often the case for thermal flow in covalent materials.[22,24] The annihilation rate of defects in the cascade then depends on defect *density*. It can only be constant for all irradiation conditions in Fig. 4 if the volume of the cascade scales proportionally with nuclear energy loss. The present experiments cannot distinguish which is the annihilation mechanism of flow defects.

In thermally activated liquids, and in some glassy materials as well, the shear viscosity η is often related to the self-diffusivity D by the Stokes–Einstein relation,[15] which states that the product ηD is constant at any given temperature. To evaluate this product for radiation-induced atomic transport, we will use the radiation-induced diffusivity which is used to describe ion-beam mixing.[12–14] For room-temperature irradiation of SiO_2, ion beam mixing can be described in terms of a purely ballistic effect,[12] and the radiation induced diffusivity is given by the phenomenological relation:

$$D_{rad} \equiv \frac{D}{\phi} = 0.067 \frac{F_n R_d^2}{\rho E_d}, \qquad (5)$$

where F_n is the energy per unit length deposited into nuclear displacements, R_d the mean range of displaced atoms, E_d the displacement energy, and ρ the atomic density. The ion flux ϕ is used to relate diffusivity D to radiation-induced diffusivity D_{rad}, analogous to the definition of η_{rad}. As can be seen, D_{rad} is proportional to F_n. From Fig. 4 it was concluded that η_{rad} is proportional to F_n^{-1}. Therefore, the Stokes–Einstein product for radiation induced atomic transport in SiO_2, $\eta_{rad} D_{rad}$, is constant, independent of ion and irradiation energy. This indicates that radiation-induced diffusion and flow are related atomic transport phenomena. Using typical values of $R_d = 10$ Å and $E_d = 15$ eV, we find $\eta_{rad} D_{rad} = 8 \times 10^{-11}$ N. This value can now be used to predict η_{rad} for cases in which D_{rad} is known, and vice versa.

Finally, Fig. 4 also shows values of η_{rad} for H and He irradiation, taken from Ref. 25, which were determined using x-ray reflectivity measurements of radiation-induced surface smoothing with ~1 keV ions. As can be seen, extrapolation of our viscosity data towards low nuclear energy loss for H and He predicts the correct order of magnitude for η_{rad}. This suggests that the flow contribution to ion-induced surface smoothing is related to the mechanism of ion beam induced flow from this work. However, the radiation-induced viscosity of H does not exactly lie on the dashed line with slope -1.1. This may be due to differences in collision cascade dimensions or a different role of the surface in the very low-energy irradiations.

3. Anisotropic deformation

In the case of the present irradiations of SiO_2 films, the stress reaches an equilibrium value after $\sim 6 \times 10^{13}$ Xe/cm^2 (Fig. 2). The final steady state is due to a dynamic equilibrium of a continuous stress generating process, and radiation-enhanced flow, which serves to relax stress.[11] Because this stress-generating phenomenon is unsaturable, it cannot be a density change but it must be a continuous anisotropic defor-
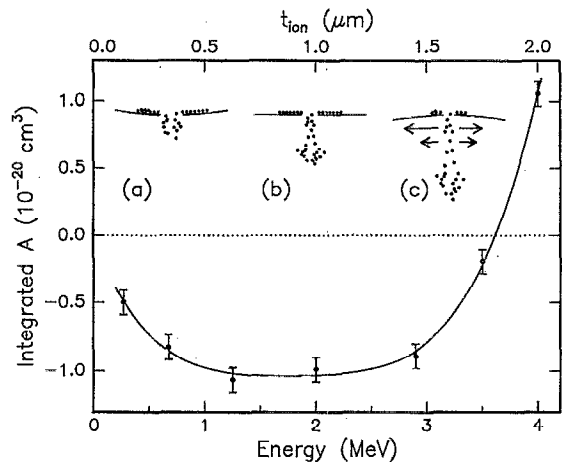

FIG. 5. Integrated deformation rate, $A \cdot t_{ion}$, as a function of Xe irradiation energy. t_{ion} is indicated on the top axis. The three insets show how the SiO_2 may react to an incoming energetic ion, for the case of low (a), intermediate (b), and high (c) energy irradiation. The solid dots represent some of the displaced atoms in the cascade. The picture for (a) is derived from a MD simulation in Ref. 26.

mation. In the case of compressive saturation stress (4.0 MeV Xe irradiation), the irradiated SiO_2 expands in-plane and therefore has to shrink normal to the plane because the density is constant;[11] for tensile in-plane saturation stress (<3.6 MeV) the opposite is the case. In absence of viscous flow, the deformation energy per unit length can be calculated using $E_{def} = Y_{ion} A$. In the case of 4.0 MeV Xe irradiation, $A = (0.57 \pm 0.15) \times 10^{-16}$ cm^2 so that $E_{def} \approx 4$ eV/nm, i.e., 0.1% of the total deposited energy for each ion is stored in the deformation.

Figure 5 shows the total deformation effect, plotted as the depth-integrated value of the deformation rate A, as a function of Xe irradiation energy. It shows the negative integrated deformation rate causing tensile stress for energies <3.6 MeV, and the positive deformation rate causing compressive stress at 4.0 MeV. In the remainder of this section, we will speculate on the interpretation of these anisotropic deformation effects in terms of a combination of a near-surface phenomenon which causes tensile stress, and a bulk process that causes compressive stress.

The insets in Fig. 5 show schematic suggestions of what would happen in the region where an ion enters the SiO_2. The insets correspond to low (a), intermediate (b), and high (c) energy irradiations. Inset (a) applies to Xe energies below 1.25 MeV. In this regime the sample becomes more curved for increasing energy, bending towards the incoming ion beam. In the direct vicinity of the track where a Xe ion enters the SiO_2, material is locally heated. This causes some atoms to be forced out of the locally hot region on to the surface, where they may condense. Material from the surrounding SiO_2 will then undergo a force to attempt to fill the vacant space that is left behind, causing a tensile stress as is observed. This idea is consistent with recent molecular dynamics (MD) simulations of 10 and 20 keV Au irradiation of Au, there the nuclear energy-loss density in the substrate is comparable to the stopping density in our experiment.[26] These MD simulations show exactly what is sketched in inset (a).
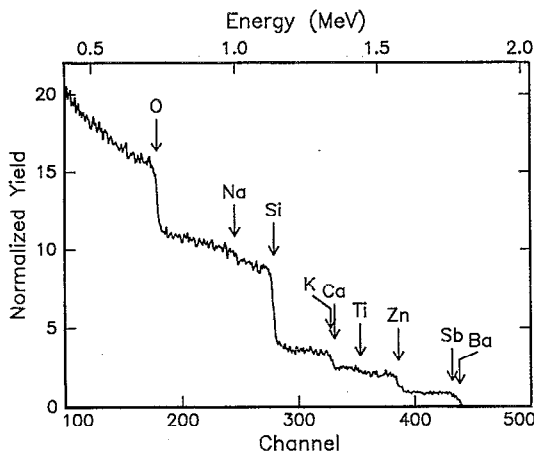
FIG. 6. RBS spectrum of the used alkali borosilicate glass (Chance CM5), taken using 2.0 MeV ^{4}He$^+$. In addition to the indicated elements, B_2O_3 is a specified ingredient.
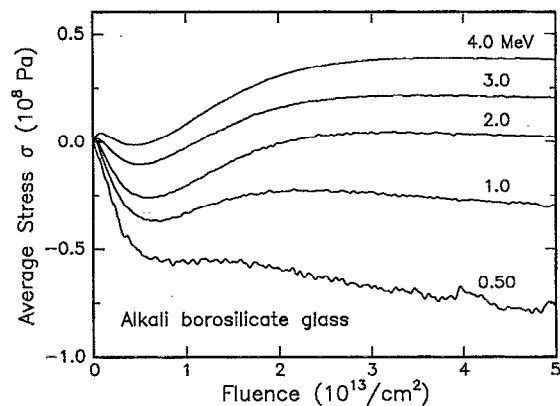

FIG. 7. *In situ* measurements of the average local stress σ of alkali borosilicate glass during irradiation with Xe at energies ranging from 0.50 to 4.0 MeV, using a constant Xe flux of 3.1×10^{10} ions/cm^2 s.

For irradiation energies above 1.25 MeV, a competing process sets in. For these energies, the electronic stopping power near the surface exceeds the nuclear energy loss. The total deposited energy density in the cascade becomes higher, and the large ion range gives rise to a more cylindrically shaped ion track [Figs. 5(b) and 5(c)]. The locally hot cylindrical region will try to expand, to relieve the thermal stress. Due to the cylindrical geometry, a net anisotropic deformation will take place, in which the material expands inelastically in the plane perpendicular to, and consequently shrinks in the direction of the cylindrical axis. This interpretation, which will lead to a compressive saturation stress, is based on a local heating effect. Earlier work on anisotropic deformation phenomena at >100 MeV energies has been interpreted in terms of a Coulomb repulsion effect of ionized atoms in SiO_2.[3,27] More recently, it has been suggested that momentum transfer from the incoming ions to the host may explain the observed deformation as well.[28]

The wafer curvature technique only yields the integrated stress, and consequently only the *integrated* deformation rate. Therefore, the net measured deformation rate is determined by the sum of the competing surface contraction and bulk expansion. At ~3.6 MeV, where the net effect of deformation on the sample curvature is zero [see Fig. 5(b)], both effects are equally strong. At 4.0 MeV the in-plane expansion effect is larger than the surface contraction effect, resulting in the situation that the sample bends away from the ion beam [Fig. 5(c)].

IV. SODALIME BOROSILICATE GLASS

A. Results

Figure 6 shows an RBS spectrum of the sodalime borosilicate used in the second series of experiments which will be described from here. The spectrum agrees with the specified composition:[29] (in wt %) 66.2 SiO_2 , 8.5 Na_2O, 1.6 CaO, 4.0 K_2O, 5.6 B_2O_3, 3.6 Al_2O_3, 1.0 MgO, 2.2 TiO_2, 4.7 ZnO, 0.7 Sb_2O_3, and 1.4 BaO. Because of the presence of heavy

elements it was not possible to determine the Xe implantation profiles with RBS; the profiles were estimated using TRIM89 code.

Figure 7 shows the average local in-plane stress in the irradiated region of this glass for Xe energies in the range 500 keV to 4.0 MeV. The average stress σ was obtained by dividing the measured integrated stress by t_{ion}=0.25, 0.48, 0.96, 1.44, and 1.90 μm, depending on Xe energy. Prior to irradiation, the bulk samples were uncurved. As the samples are implanted above 1.0 MeV, the stress first shows a slight but rapid increase within the first ~10^{12} ions/cm^2. The average stress then decreases, after which it increases again to finally saturate after ~3×10^{13} Xe/cm^2. For 4.0 MeV Xe irradiation, the saturation stress is $(0.39 \pm 0.04) \times 10^8$ Pa, compressive. The saturation stress decreases with irradiation energy, turning tensile below 2.0 MeV. For 500 keV the tensile saturation stress is $-(0.8 \pm 0.2) \times 10^8$ Pa. Apart from the initial transient, the behavior in Fig. 7 is qualitatively similar to that observed for pure silica in Fig. 2.

Figure 8 shows the integrated in-plane stress S of the alkali-borosilicate glass during irradiation with 4.0 MeV Xe
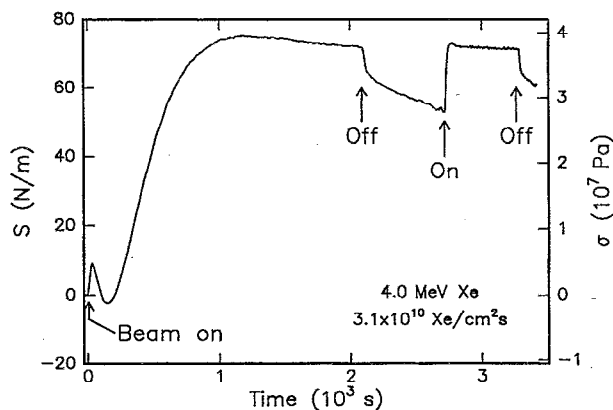

FIG. 8. Integrated stress of sodalime borosilicate glass during irradiation with 4.0 MeV Xe as a function of time. The beam was first switched on at $t=0$. At certain moments, the ion beam with a flux of 3.1×10^{10}/cm^2 s was stopped and switched on again.
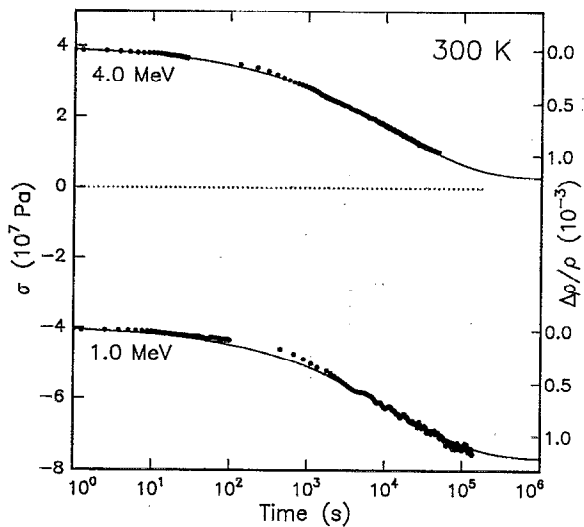
FIG. 9. Evolution of the average stress after the beam was switched off. Data are plotted as a function of time on a logarithmic scale. The sodalime borosilicate glass was first irradiated to the saturation stress, using 7×10^{13} Xe/cm² at 4.0 or 1.0 MeV. The drawn lines are fits to a stretched exponential function.

FIG. 10. Integrated stress measured after the 4.0 MeV Xe beam was switched on. The sample was first irradiated with 7×10^{13} Xe/cm², causing saturation of the stress; then the beam was stopped, and the sample was relaxed to $S=60$ N/m. Dose rates of 1.6 and 3.1×10^{10} ions/cm² s were used.

as function of time. At $t=0$ the irradiation starts, with a constant flux of 3.1×10^{10} ions/cm² s. The curve evolves as described above, until the beam is switched off after 2.1×10^3 s, corresponding to a fluence of 6.5×10^{13} ions/cm². It can be seen that the stress then decreases, first rapidly and then more slowly. This is an important difference compared to the results for SiO₂, where the stress remained at the same level as the beam was switched off. When the ion beam is switched on again, the stress increases very rapidly, and returns to the value it had before stopping the irradiation within a fluence of 2×10^{12} ions/cm². A similar behavior is seen when the ion beam is switched off a second time.

Figure 9 shows the stress decrease after the ion beam was stopped in more detail, and over a longer time scale than in Fig. 8. The data are plotted as a function of time on a logarithmic scale for up to 40 h. Two cases are shown: one after irradiation with 1.0 MeV Xe, which yields a tensile saturation stress, and one after irradiation with 4.0 MeV Xe which starts at a compressive saturation stress. In both cases the stress continues to become more tensile for times as long as 40 h. As can be seen, neither the time evolution nor the total change in average stress depends on the preceding irradiation energy, or the sign and magnitude of the stress.

The "beam on" behavior is shown in more detail in Fig. 10 for two 4.0 MeV Xe fluxes of 1.6 and 3.1×10^{10} ions/cm² s, as a function of fluence. In both cases the beam was switched on after the stress had first relaxed to 60 N/m. As can be seen, the final saturation stress is equal for both irradiation fluxes. A small overshoot is seen for a flux of 3.1×10^{10}/cm² s before reaching equilibrium, whereas for the lower flux the rapid initial stress increase is followed by a slow approach to the equilibrium value. The fact that the same saturation stress is reached for both fluxes indicates that the curvature increase as the beam is switched on is not due to macroscopic beam heating of the sample surface.
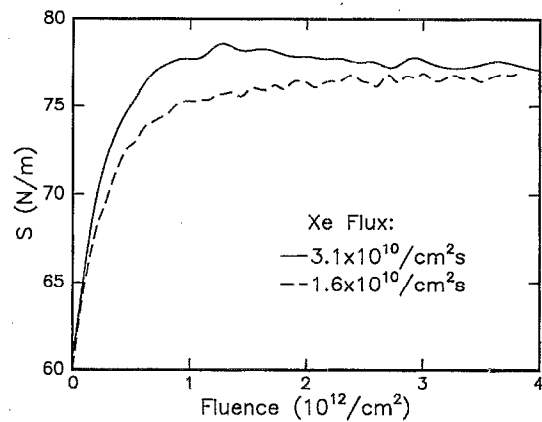
B. Analysis and discussion

The most important difference between the stress evolution in the multicomponent glass compared to the behavior in the SiO₂ case (Sec. III), is the transient behavior as the beam is switched on or off. Figure 9 shows that the direction and magnitude of the stress change as the beam is switched off, is independent of the initial stress (compressive or tensile) or ion energy with which the sample was irradiated. Therefore this stress change can not be described in terms of viscous flow, as this can only cause relaxation of stress to zero. In fact, the observation that the absolute stress change as a function of time is identical for both curves implies that the stress changes shown in Fig. 9 are purely a result of structural relaxation.[30] Structural relaxation may result in a density increase due to the annihilation of volume occupying (point) defects, causing a more tensile stress, as is observed. In the following we will refer to these defects as δ defects. The relative density change can be extracted from the change in average in-plane stress by[8]

$$\frac{\Delta\rho}{\rho} = -\frac{3\Delta\sigma}{Y_{\text{ion}}}, \tag{6}$$

where ρ is the density of the damaged region as the ion beam is switched off. The relative density increase, according to this interpretation, is shown on the right-hand axis in Fig. 9; after 40 h the material has densified by almost 0.12%. This number is in the same range as the observed density decrease of α-quartz due to the creation of E' centers (oxygen vacancies).[2,31] Therefore, the long-time structural relaxation in irradiated alkali borosilicate glass may be due to the annihilation of such vacancies. The room-temperature annihilation of δ defects may be related to the presence of alkali cations, which are mobile in the network at low temperatures. It is also known that alkali atoms become more mobile during irradiation, and at much higher fluences ($\sim10^{15}$/cm²) than used in our experiments, they even show macroscopic depletion below the surface.[32,33] It is interesting to note that
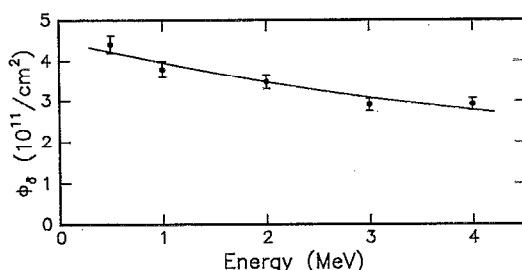
FIG. 11. Characteristic ($1/e$) fluences ϕ_δ at which the stress changes to the saturation level as the beam is switched on, as a function of Xe beam energy. ϕ_δ is obtained by fitting exponential functions to data like in Fig. 10.

the δ defects do not have a large effect on the viscosity of the glass, as no significant viscous flow is observed during the annihilation period of these defects (Fig. 9).

Properties related to structural relaxation in glasses can often be described with a stretched exponential function $\Delta\rho/\rho \propto 1 - \exp[-(t/\tau)^\beta]$. A fit, yielding $\tau = (12.2 \times 1.7) \times 10^3$ s and $\beta = 0.40 \pm 0.16$ is shown by the solid lines in Fig. 9. Stretched exponential behavior indicates that the relaxation is governed by a distribution of relaxation times,[30] which means that the activation energies of the processes that contribute to the density increase are distributed over a continuous spectrum.[34,35] This is a common feature for structural relaxation in amorphous materials like oxides[30] and in amorphous Si.[36] In an isothermal annealing experiment, the time axis reflects the activation energies: at temperature T, relaxation processes with activation energies lower than $Q = kT \ln(\nu t)$ (ν is an attempt frequency) have taken place at time t.[34] Thus, in case of a flat spectrum of activated processes, the measured property behaves linearly as a function of $\ln(\nu t)$. However, the data in Fig. 9 show a clear change in slope at $t \approx 2.0 \times 10^2$ s. Assuming an attempt frequency $\nu = 10^{12}$ s^{-1}, this corresponds to a sharp change in the defect annihilation kinetics at $Q = 0.7$ eV. This can be a difference in the density of processes with activation energy above or below 0.7 eV, or a difference in the nature of the defects.

Finally, the data in Fig. 10 can be used to obtain information on the creation mechanism of the δ defects. The equilibrium stress value is independent of ion flux. This is due to the fact that once volume changes have saturated, radiation-enhanced flow always relaxes the stress to the saturation value of $6A \eta_{rad}$, independent of density. We fitted an exponential function $S_0 + (S_{sat} - S_0)(1 - \exp[-\phi/\phi_\delta])$ to the curves in Fig. 10 between 0 and 1.5×10^{12} Xe/cm^2. For both curves this yields $\phi_\delta = 2.6 \times 10^{11}$/cm^2, whereas the fluxes at which the curves were measured differ a factor of 2. This means that the creation rate (in s^{-1}) of the defects is proportional to the ion flux.

The dependence of ϕ_δ on Xe irradiation energy is shown in Fig. 11. Irradiations were performed at energies in the 0.5–4.0 MeV range. The silica was first irradiated to a high enough fluence to reach the saturation stress. Then the beam was stopped in order to let the sample stress decrease, and subsequently switched on again in order to determine ϕ_δ. As can be seen, the δ defects are created faster at higher beam energy. The average electronic energy loss in Fig. 11 in-

creases with energy, whereas the average nuclear energy loss is almost constant in the 0.5–4.0 MeV energy range. Electronic energy-loss processes therefore contribute to the creation of δ defects. This is not unusual for density changes in alkali silicates.[37] The energy dependence of ϕ_δ is opposite to that observed for ϕ_p [Fig. 3(b)] for densification, which is known to scale predominantly with nuclear energy loss.[1,2,8] This indicates that the density changes due to network compaction are not related to the density changes due to the creation of δ defects. This is consistent with what is known about E' centers.[2]

The complete development of the stress in the multicomponent glass (shown in Figs. 7 and 8) can now be understood by a combination of four different processes: *densification* of the silica network, radiation-enhanced *viscous flow*, *anisotropic deformation*, and the creation of *volume occupying δ defects*. When the ion beam is first switched on, δ point defects are produced at a relatively high rate, resulting in a small compressive stress (initial increase in Fig. 8). However, at the same time densification of the ring network takes place whereby the glass network is transformed into a more compact state. When the concentration of the δ defects reaches a steady state (i.e., after 20 s in Fig. 8), a net stress decrease is observed due to the ongoing densification. After 0.5×10^{13} ions/cm^2, see Fig. 7, the net in-plane stress is increasing again (except for the 500 keV data). At this point the network densification has saturated, and no more density changes occur. The stress increase is explained by the net effect of the beam-directional anisotropic deformation and viscous flow. Finally, a saturation stress is reached, determined by the balance of the rates of anisotropic deformation and viscous flow: $\sigma_{sat} = 6A \eta_{rad}$.

The radiation-induced viscosity η_{rad} can be extracted from the data in Fig. 7 by fitting an exponential [see Eq. (3)] through the part of the data that is mainly determined by viscous relaxation, i.e., at fluences above 1.5×10^{13} Xe/cm^2. This yields $\eta_{rad} = (0.95 \pm 0.10) \times 10^{23}$ Pa ions/cm^2. This value is almost the same as found for pure SiO$_2$ in Sec. III. At a flux of 3.1×10^{10} ions/cm^2 s it corresponds to a viscosity $\eta = 3.1 \times 10^{12}$ Pa s. This is comparable to the specified thermal viscosity of the alkali borosilicate glass at 550 °C. The specified transformation temperature for this glass is 573 °C.[29]

Using $\eta_{rad} = 0.95 \times 10^{23}$ Pa ions/cm^2, the anisotropic deformation rate A can be extracted from the saturation stresses in Fig. 7, and ranges from $-(1.4 \pm 0.4) \times 10^{-16}$ to $+(0.667 \pm 0.018) \times 10^{-16}$ cm^2 for energies ranging from 0.5 to 4.0 MeV. The magnitude of A and its general behavior as a function of energy are very similar to that for pure SiO$_2$. This implies that the deformation phenomena are a general feature for silica glasses. In fact, these effects may be important in other materials (other glasses, semiconductors) as well.

V. TECHNOLOGICAL IMPLICATION

The results of this study have important consequences for mask applications in high-energy heavy-ion implantation. As an example we will show results of 4.9 MeV Er implantation in sodalime silicate glass at room temperature. Prior to
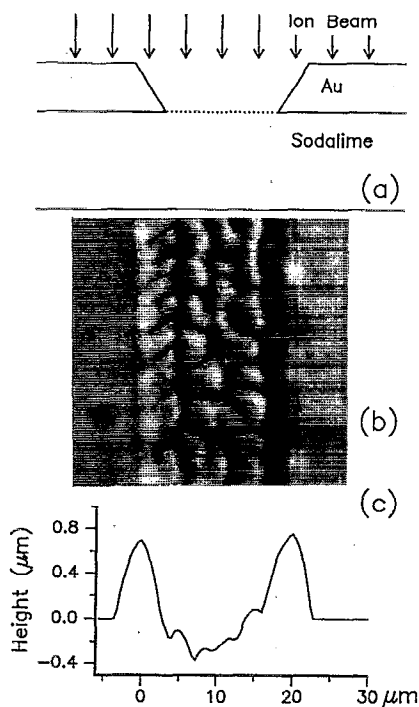
FIG. 12. (a) Schematic cross section of a Au contact mask with a trench on sodalime glass. (b) Top view of the implanted glass after etching off the Au mask as seen with an optical microscope. (c) Surface profile measured perpendicular to the trench after etching off the Au mask.

implantation, a 1.0-μm-thick gold layer was deposited, after which photolithography and etching was used to define 15-μm-wide trenches in the Au to create a contact mask [Fig. 12(a)] thick enough to fully stop 4.9 MeV Er ions. After irradiation with 3×10^{16} Er/cm^2, the gold was etched off. Figure 12(b) shows a top view of an implanted stripe. The irradiated surface is very rough. The surface height across the implanted region is shown in Fig. 12(c), and shows 0.6-μm-high rims of material accumulated along the inside of the Au mask, as well as considerable roughness within the rims.

The accumulation of material along the sides of the implanted regions is consistent with the anisotropic deformation effect that is shown to be present during MeV heavy-ion irradiation. After densification, the material in the bombarded region undergoes the anisotropic expansion in directions perpendicular to the ion beam, but is constrained on both sides of the trench by glass that is not irradiated. The only way to relax stress in the irradiated region is then to build up on the sides.

The roughness observed within the trench is attributed to the combined effect of expansion, sputtering, surface diffusion, and plastic flow. The surface roughness seems similar to roughening effects seen during low-energy irradiation.[25]

When such an implantation is used for doping of optical waveguides, this roughness will cause very high and undesirable optical losses due to scattering. Finally, we remark that deformation of silica implantation masks[11] and roughening of silica surfaces is significantly reduced when the implantation is performed around 300 °C. This may be a result of a decrease in the radiation-induced viscosity, in combina-

tion with a possible temperature dependence of the anisotropic deformation phenomenon.[4] The temperature dependence of η_{rad} and A is currently under investigation.

VI. CONCLUSIONS

When silica glass is ion irradiated at energies of the order of 1 MeV, three effects are observed: densification, anisotropic deformation, and radiation-enhanced viscous flow. Using an empirical model, parameters that describe these processes were obtained.

The radiation-induced viscosity is inversely proportional to the nuclear energy loss over a range of at least two orders of magnitude. The product of the radiation-induced viscosity and ballistic diffusivity is constant: $\eta_{rad} D_{rad} = 8 \times 10^{-11}$ N, in an analogous way as in the Stokes–Einstein relation for thermally activated fluids. The data can be used to predict η_{rad} and D_{rad} for a large variety of irradiation conditions. The anisotropic deformation results in a compressive stress at high (>3.6 MeV Xe) energies, and in a tensile stress for lower ion energies. These effects are explained in terms of competing bulk and surface deformation processes resulting from local heating of the SiO$_2$ around the ion tracks. For 4.0 MeV Xe, at most 0.1% of the incident ion energy is stored into deformation energy.

A fourth irradiation-induced phenomenon is observed in a multicomponent alkali borosilicate glass, and is related to the presence of the high density of network modifiers, such as Na. It shows density changes up to 0.12%, attributed to irradiation-induced volume occupying point defects, which may be oxygen vacancies (E' centers). Electronic energy-loss processes contribute to the creation of these defects. The defects anneal out at room temperature, according to a broad spectrum of activation energies.

[1] W. Primak, Studies in Radiation Effects in Solids (Gordon and Breach, New York, 1975), Vol. 4.
[2] R. A. B. Devine, Nucl. Instrum. Methods B 91, 378 (1994).
[3] S. Klaumünzer, Radiat. Eff. 110, 79 (1989).
[4] A. Benyagoub, S. Löffler, M. Rammensee, and S. Klaumünzer, Nucl. Instrum. Methods B 65, 228 (1992).

J. Appl. Phys., Vol. 78, No. 7, 1 October 1995

Snoeks et al.   4731

[5] A. Polman, D. C. Jacobson, D. J. Eaglesham, R. C. Kistler, and J. M. Poate, J. Appl. Phys. **70**, 3778 (1991).

[6] E. Snoeks, G. N. van den Hoven, and A. Polman, J. Appl. Phys. **73**, 8179 (1993).

[7] E. Snoeks, G. N. van den Hoven, A. Polman, B. Hendriksen, M. B. J. Diemeer, and F. Priolo, J. Opt. Soc. Am. B **12**, (1995) (in press).

[8] E. P. EerNisse, J. Appl. Phys. **45**, 167 (1974).

[9] W. Primak, J. Appl. Phys. **35**, 1342 (1964).

[10] C. A. Volkert and A. Polman, Mater. Res. Soc. Symp. Proc. **235**, 3 (1992).

[11] E. Snoeks, A. Polman, and C. A. Volkert, Appl. Phys. Lett. **65**, 2487 (1994).

[12] W. Bolse, Mater. Sci. Eng. R **12**, 53 (1994).

[13] M. Nastasi and J. W. Mayer, Mater. Sci. Eng. R **12**, 1 (1994).

[14] Y.-T. Cheng, Mater. Sci. Rep. **5**, 45 (1990).

[15] See for instance: P. A. Egelstaff, *An Introduction to the Liquid State* (Oxford University, Oxford, 1992), Chap. 13.

[16] C. A. Volkert, J. Appl. Phys. **70**, 3521 (1991).

[17] W. A. Brantley, J. Appl. Phys. **44**, 534 (1973).

[18] H. Scholze, *Glass* (Springer, Heidelberg, 1990).

[19] J. P. Biersack and L. J. Haggmark, Nucl. Instrum. Methods **174**, 257 (1980).

[20] J. Heibei and E. Voges, Phys. Status Solidi **57**, 609 (1980).

[21] N. F. Mott, Philos. Mag. B **56**, 257 (1987).

[22] H. R. Lillie, J. Am. Ceram. Soc. **16**, 619 (1933).

[23] S. S. Tsao and F. Spaepen, Acta Metall. **33**, 881 (1985).

[24] A. Witvrouw and F. Spaepen, J. Appl. Phys. **74**, 7154 (1993).

[25] T. M. Mayer, E. Chason, and A. J. Howard, J. Appl. Phys. **76**, 1633 (1994).

[26] M. Ghaly and R. S. Averback, Phys. Rev. Lett. **72**, 364 (1994).

[27] S. A. Fedotov, V. S. Varichenko, A. M. Zaitsev, M. Ishimaru, Y. Hiroyama, and T. Motooka, Mater. Sci. Eng. B **29**, 202 (1995).

[28] L. Cliche, S. Roorda, M. Chicoine, and R. A. Masut (private communication).

[29] Data sheets for Microscope Coverslip glass CM5, Change Propper Ltd., Warley, England.

[30] G. W. Scherer, *Relaxation in Glass and Composites* (Wiley, New York, 1986).

[31] K. Tanimura, T. Tanaka, and N. Itoh, Phys. Rev. Lett. **51**, 423 (1983).

[32] P. Mazzoldi and G. W. Arnold, in *Ion Beam Modification of Insulators*, edited by P. Mazzoldi and G. W. Arnold (Elsevier, Amsterdam, 1987), Chap. 5.

[33] G. W. Arnold, Nucl. Instrum. Methods B **1**, 516 (1984).

[34] M. R. J. Gibbs, J. E. Evetts, and J. A. Leake, J. Mater. Sci. **18**, 278 (1983).

[35] W. Primak, Phys. Rev. **100**, 1677 (1955).

[36] S. Roorda, W. C. Sinke, J. M. Poate, D. C. Jacobson, S. Dierker, B. S. Dennis, D. J. Eaglesham, F. Spaepen, and P. Fuoss, Phys. Rev. B **44**, 3702 (1991).

[37] G. W. Arnold, Radiat. Eff. **98**, 221 (1986).